SOME RESEARCH ON CONTROL OF VIBRATIONS IN CIVIL ENGINEERING UNDER COVICOCEPAD PROJECT

R.C. Barros[1], A. Baratta[2], O. Corbi[2], M.B. César[1], M.M. Paredes[1]

[1] FEUP – Faculdade de Engenharia, Universidade do Porto (UP), Portugal
  Department of Civil Engineering, Rua Roberto Frias, 4200-465 Porto, Portugal
   Email: rcb@fe.up.pt , dec05002@fe.up.pt , dec08014@fe.up.pt

[2] University of Naples Federico II, Naples, Italy
  Department of Structural Engineering, via Claudio 21, 80125 Napoli, Italy
   Email: Alessandro.baratta@unina.it , ottavia.corbi@unina.it

SYNOPSIS

Some information is provided on the latest R&D within COVICOCEPAD project approved in the framework of Eurocores program. It addresses the use of TMD's TLD's, base isolation devices, MR dampers and a hybrid technique using both devices together. Some results are provided associated with calibration of a MR damper at FEUP, as well as its inclusion in a small scale laboratory set-up with proper equations of motion of the controlled smart structure. Applications of TMD's devices to two civil engineering structures under dynamic and seismic actions are also outlined.

INTRODUCTION

In the last two decades R&D of structural vibration control devices for buildings and bridges has been intensified to reply to construction market needs that demand more effective systems to decrease the damage caused by seismic and wind loading. This orientation is the result of a public necessity to guarantee the serviceability of construction lifelines throughout and after the occurrence of a moderate or severe seismic event (Barros *et al* [1] [2]).

The COVICOCEPAD project earlier objectives and preliminary works, on TLD's and on algorithm strategies for semi-active control, have already been reported by Barros [3] [4], Barros and Corbi [5] [6], Guerreiro, Barros and Bairrão [7], among others [8] [9] [10] [11].

Herein in the sequel of contract and financial support only initiated in November 2007, which only then allowed organized contacts for potential researchers and the warranted request for the supply of a Quanser shake table II (QST-II) delivered in November 2008, the project leader and the local team coordinators synthesize part of the ongoing R&D in the project thematic. The QST at FEUP (Porto) was calibrated, from Dec 2008 until March 2009, with the adequate use of the supplied 2-DOF frame equipped with 2 passive/active TMD devices. Future collective work will detail experimental results obtained with QST at FEUP and their analytical modelling, also theoretical developments at both University of Naples (Federico II) and IST (Lisbon), as well as larger scale tests using vibration damper devices at a LNEC (Lisbon) steel frame under the same project.

Two very recent publications under COVICOCEPAD project (Barros, Baratta et al. [12], Paredes, Barros and Cunha [13]) emphasize part of the collective work of the international research team.

PASSIVE CONTROL OF STRUCTURAL VIBRATIONS

Passive Control using Base Isolation (BI)

In the last two decades R&D of structural vibration control devices for buildings and bridges has been intensified to reply to the construction market needs that demand more effective systems to decrease the damage caused by a seismic and wind loading. This orientation is the result of a public necessity to guarantee the serviceability of construction lifelines after and throughout the occurrence of a moderate/severe seismic event.

In this context, the strategies based on the passive control, namely the base isolation (BI) systems, shock absorbers (SA) and tuned mass dampers (TMD) are well-known and accepted methodologies due to its effectiveness as mitigation approach for dynamic loading. However, the limitations that these devices/methodologies have to allow variations of the dynamic loading or structural parameters encouraged the study and development of more advanced control systems based on active, semi-active or hybrid control devices (Figure 1).
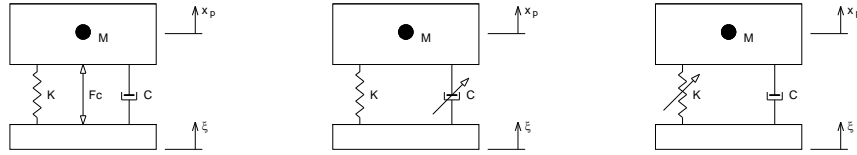

Figure 1: Active and semi-active vibration control strategies.

The numerical models used to simulate this new type of control in civil engineering structures allows to conclude that is possible to apply them successfully but some experimental research is requested to validate these models in order to be accepted as a possible structural vibration control solution. Since active devices are not a practical and reliable option in the near future as a structural building or bridge control systems due to energy demand and possible failure in case of power loss, semi-active control devices gain significant attention by the civil engineering community in the last years because they have at the same time the benefits of passive and active devices without requiring a huge amount of energy to properly work.

The easiest and cheapest way to protect a structure from undesired vibration is to add a passive isolation system to reduce the response in some sensitive region. Figure 2 shows a single degree-of-freedom isolator, modelled by the transmissibility transfer function:

$$T = \frac{x_p}{x_b} = \frac{\dot{x}_p}{\dot{x}_b} = \frac{\ddot{x}_p}{\ddot{x}_b} = \frac{1 + 2\xi_p \dfrac{s}{\omega_n}}{1 + 2\xi_p \dfrac{s}{\omega_n} + \dfrac{s^2}{\omega_n^2}} \tag{1}$$

where s is the Laplace variable, ω_n is the natural frequency, ξ is the passive damping ratio, x_p and x_b are the payload and base displacements. The transmissibility modulus and phase for several damping ratios are also shown in Figure 2. In this figure is visible that at low passive damping ratios, the resonant transmissibility is relatively large while at frequencies above resonant peak is quite low and the reverse is true for relatively high damping ratios.

The base isolation system is the first approach in the analysis of structures with passive energy dissipation devices and is based on the use of a model with 2 (translational) DOF represented in Figure 3.
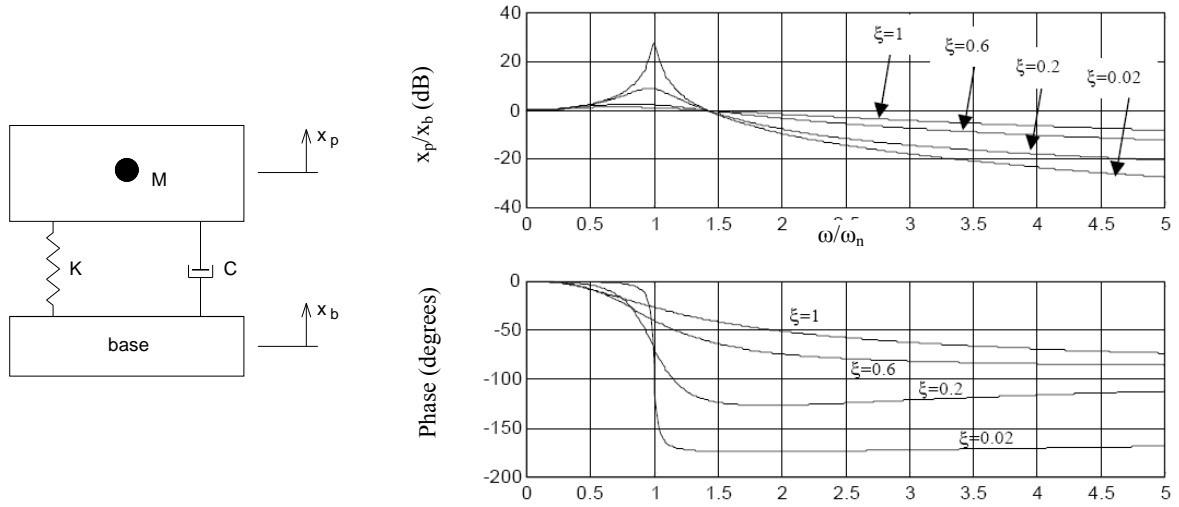
Figure 2: Passive 1-DOF isolator and transmissibility transfer function.

The background to this work was based on Naeim and Kelly [14] and Soong and Dargush [15] that resumes the theory of seismic isolation and the design of seismic isolated structures, within the framework of existing codes. In this context such model was used earlier by Barros and Cesar [16] , Cesar and Barros [17]. Also Figueiredo and Barros [18] have addressed the importance of the influence of increasing damping in seismic isolation.
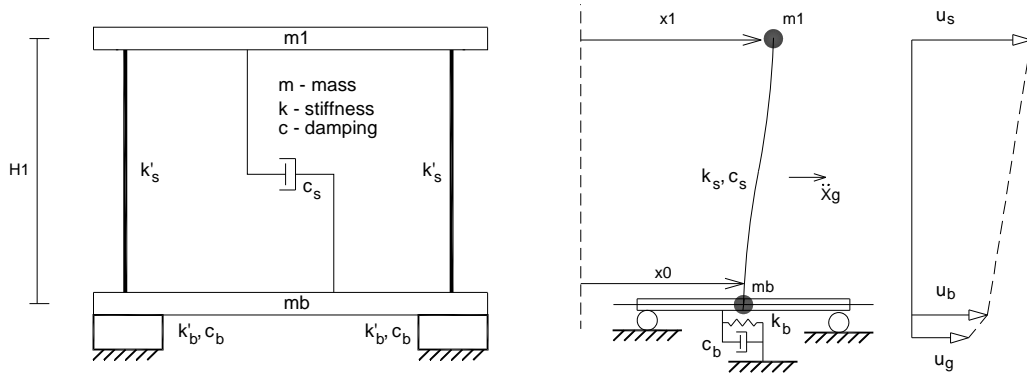

Figure 3: Passive energy dissipation at the base of the structure (Base Isolation).

The classical design approach for the base isolation devices accounting horizontal seismic component is also shown in Figure 3. In this case the equation of motion (2) has the matrix identifications (mass, damping and stiffness matrices) given in equation (3), where c_b is the damping coefficient of the isolation system, c_s is the damping coefficient of the fixed structure and k_s is the stiffness of the fixed-base structure.

$$M\ddot{X}(t) + C\dot{X}(t) + KX(t) = -M\{I\}a(t) \qquad (2)$$

$$M = \begin{bmatrix} m_b & 0 \\ 0 & m_1 \end{bmatrix}, \ C = \begin{bmatrix} c_b + c_s & -c_s \\ -c_s & c_s \end{bmatrix}, \ K = \begin{bmatrix} k_b + k_s & -k_s \\ -k_s & k_s \end{bmatrix} \qquad (3)$$

Base isolation devices are made of natural rubber that guarantees damping ratios in the order of 10-20% of critical damping, considerably bigger than structural damping ratios for steel frames (in the order of 2%).

In our study a vibration absorbing mounting similar to those used for machine isolation is used to simulate the base isolation system. Because this simplified passive system has an insignificant energy dissipation – an important characteristic for real building applications – the expected structural behaviour remains the same as for a real base system; so the main purpose of a base isolation system is to increase the structural flexibility and consequently the main period to a more secure range, in which resonance effects are significantly lower (and often irrelevant) becoming a type of pseudo-filter [2] [16] [17].

Actually the final skill of base-isolation devices for structural applications in mitigating inertia forces due to intense earthquakes, strongly depends on the proper calibration of the isolator own frequency, which should be carefully dimensioned taking into account both the dynamical characteristics of the superstructure and the frequency content of the expected disturbance (Baratta and Corbi [19] [20]). Surface layers of the ground on which the building is founded have the capacity of filtering the incoming dynamic excitation making its signal dependent on the characteristics of the soil.

Therefore, in designing a base isolator system, one should not neglect the interaction effects between the structure itself and the soil characterizing the site, since the soil behaves like a filter as regards to the incoming seismic excitation, mainly affecting its frequency composition and, definitively, its overall dynamic character.

At the Department of Structural Engineering of the University of Naples Federico II, a strategy for designing an effective isolation device on the basis of the knowledge of the structure mechanical characteristics and of the soil properties has been developed, imposing that the desired isolator behaviour is such to minimize the energy introduced in the structure by the dynamic excitation, while allowing a bounded energetic absorption in the isolator itself, lower than a prefixed threshold.

The adoption of this approach requires, of course, the evaluation of the energies characterizing the structure $\mathcal{E}_{str}(\omega \mid \eta, \xi)$ and the base isolation device $\mathcal{E}_{is}(\omega \mid \eta, \xi)$ during the seismic motion, as functions of the varying isolator characteristics m_{is}, c_{is}, k_{is}, and of the soil properties η and ξ; these energies can be obtained by referring to the integrals of the relevant auto-spectral density terms.

The search of the isolator parameters can be pursued by requiring that the energy absorbed by the structure is minimum while the energy introduced in the isolator is kept bounded, by setting up the problem:

$$\text{Find} \quad \min_{m_{is}, c_{is}, k_{is}} \mathcal{E}_{str}(\omega \mid \eta, \xi)$$

$$\text{Sub} \quad \begin{cases} \mathcal{E}_{is}(\omega \mid \eta, \xi) \leq \overline{\mathcal{E}}_{is} \\ m_{is} \geq \overline{m}_{is} \end{cases} \qquad (4)$$

In Equation (4) one can observe the presence of two constraints, one being the mentioned bound on the isolator energy absorption $\overline{\mathcal{E}}_{is}$, the other being a practical bound on the minimum value of the isolator mass $\overline{m}_{is}$. Numerical investigation developed at the University of Naples on base isolated shear-type structures, subject to accelerations compatible with the Kanai-Tajimi spectra with assigned parameters η and ξ, allow to observe that in the cases when the soil is already very soft (mean square ratio higher than one) or poorly stiff (mean square ratio approximately one) with comparison to the structure, the isolator is not useful.

In Figure (4) one reports the time response of the optimal isolator $x_1(t)$ and of the optimally isolated superstructure $x_2(t)$, for a base isolated SDOF shear frame subject to a base acceleration compatible with a Kanai-Tajimi spectrum with parameters $\eta = 5$ sec^{-1} and $\xi = 3$.
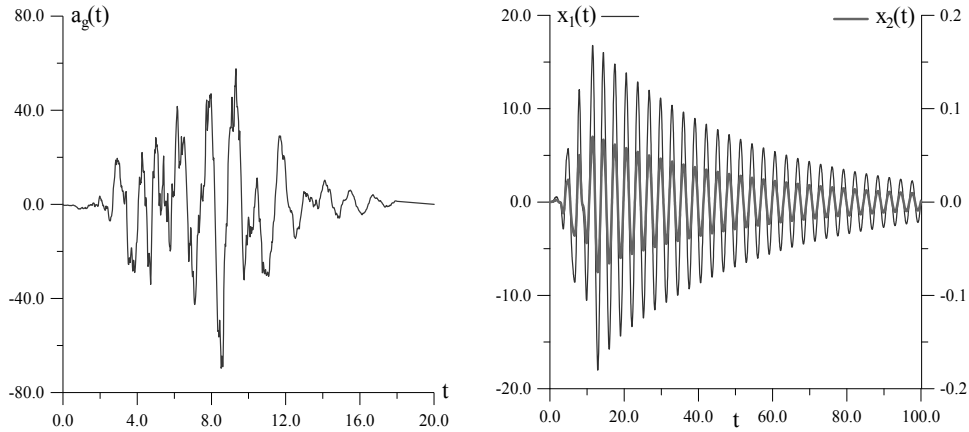

Figure 4: (a) Base acceleration compatible with the Kanai-Tajimi spectrum with $\eta = 5$ sec^{-1} and $\xi = 3$.
(b) Time response of the isolated structural system.

Synthetic results on the same structure while varying the isolator mechanical characteristics in terms of ω_1 and ζ_1 are diagrammed in Figure (5), where the maximum response values attained by the isolation device and by the superstructure are reported.

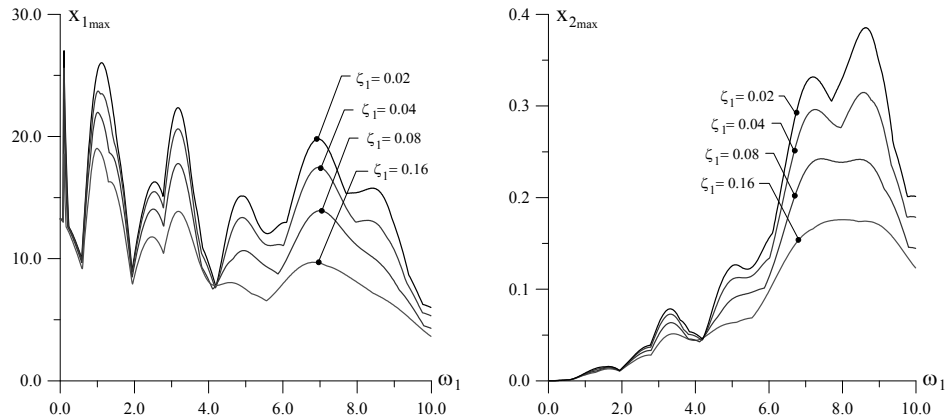Figure 5: Curves of the maximum drifts attained during the motion by varying isolator parameters ω_1 and ζ_1:
(a) isolator; (b) superstructure.

Passive Control using Tuned Liquid Dampers (TLD)

Among the many vibration control devices available to increase the damping characteristics of the structures, tuned liquid dampers (TLD) offer several advantages, namely: low cost, easiness to install in existing structures and effectiveness even for small-vibrations (Kareem [21], Corbi [22], Barros and Corbi [5] [6], Barros [23]).

The performance of TLD relies mainly on the sloshing of liquid at resonance to absorb and dissipate the vibration energy of the structure. The liquid is contained in partially filled tanks mounted on the structure. The shear force F_{TLD} caused by the inertia of the liquid mass reduces the structural response due to the excitation action F_g (Figure 6).

Tuning the natural frequency of liquid sloshing with the natural frequency of structure, results in the optimization of the effectiveness of the damper.
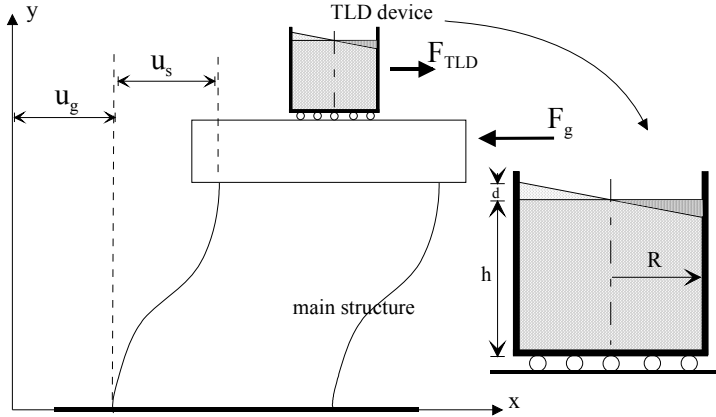

Figure 6: SDOF shear frame equipped with TLD device.

Theoretical models of liquid sloshing in TLD can be obtained either from a mechanical analogue, or from more exact analytical models of the structural and liquid domain. Actually the reliable prediction of dynamic response of control devices based on fluid motion plays a central role for better understanding the real perspectives offered by TLD for applications in the field of intelligent structures, as regards to mitigation of earthquake and vibration hazards through vibration control.

The need of predicting and preventing failures associated to rocking and overturning of rigid structures undergoing strong ground shaking have motivated a consistent number of studies on rocking response of rigid blocks, and the possibility of coupling sloshing devices for attenuating their rocking response to dynamic excitations appears pretty interesting.

Laboratory tests developed at the Laboratory of the Department of Structural Engineering of the University of Naples on metallic blocks (Figure 7) equipped with sloshing dampers prototypes and located on a shaking table show the potential benefits produced by these devices in attenuating the primary model response (Kareem [21]).
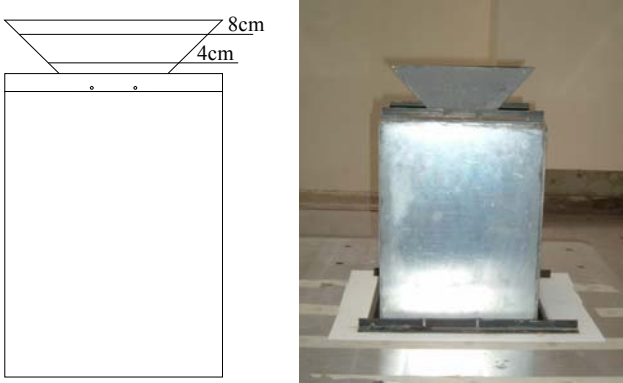

Figure 7: Block equipped with 45° tank marked at two liquid levels (4 cm and 8 cm).

Experimental data in Figures 8-10 show that significant beneficial effects can be produced in the attenuation of the rocking motion.

Such attenuation is quite clear, for example, from the diagram of the curves depicting the empty/full ratio for the model equipped with a trapezoidal tank (Figure 7): the ratio between the model responses for the empty tank and for the tank filled with 4 cm or 8 cm of water shows the performance of the device, whose effectiveness is mainly lumped on a given frequency range. As it appears, the level of the liquid in the tank is able to deeply change the characteristics of the device and, therefore, its overall response.

The effectiveness of the device can be appreciated by comparison with the unit-ratio line. Time histories also confirm the advantage of adopting such devices in the considered frequency range, showing a good mitigation of the dynamical response of the primary model.
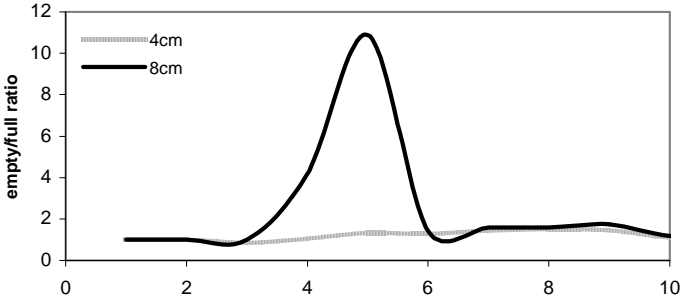

Figure 8: Block 30×30×40 cm equipped with a trapezoidal tank.
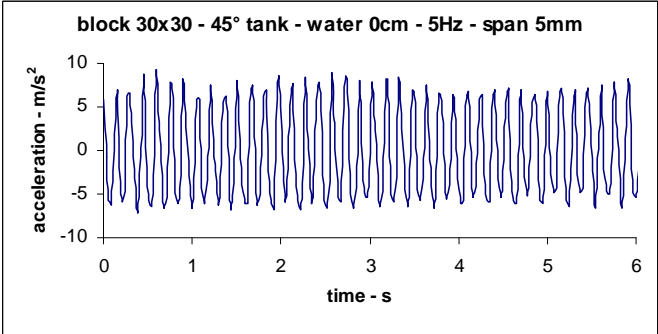

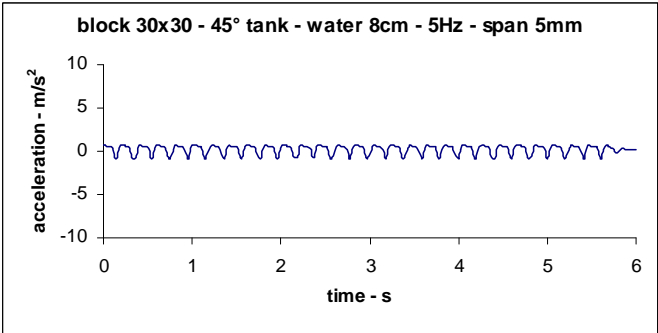Figure 9: Block 30×30×40 cm equipped with a trapezoidal (45°) empty tank.

Figure 10: Block 30×30×40 cm equipped with a trapezoidal (45°) tank filled with 8cm of water.

Presently a novelty model tank, multi-partitioned in 1-2-3-4-9-16 equal tanks, is being tested at FEUP using the QST-II of the COVICOCEPAD laboratory. Equivalent viscous damping coefficients will be determined for different heights of sloshing liquid. Also the 2-DOF Quanser frame will be tested with TLD devices to characterize its performance.

7

Passive Control using Tuned Mass Dampers (TMD)

TMD Applications to Buildings under Earthquakes

This study is a parametric analysis of the performance of a TMD in the mitigation of the effects of earthquakes in building-like structures. The targeted parameters in the analyses were the number of storey's of the buildings, the mass ratio μ of the TMD, and the earthquake input signals. The number of storey's of the buildings varied from 5 to 30 with increments of 5 storey's. The mass ratio of the TMD varied from 0.00 to 0.05 with increments of 0.01. The actions considered were the 1951 El Centro earthquake and the 1995 Kobe earthquake.

One of the objectives of this study was trying to determine or suggest an optimum range of values of μ. The design procedure of a TMD to face seismic excitations is based in equation (5) that was developed by Villaverde in [24].

$$|\xi_S - \xi_T| = |\phi_k \sqrt{\mu}| \qquad (5)$$

where ξ_S is the damping ratio of the structure, ξ_T is the damping ratio of the TMD, ϕ_k is the amplitude of the component of the mode shape to be controlled corresponding to the degree of freedom where the tuned mass damper will be installed and μ is the ratio of the TMD mass to the modal mass of the structure. It is important to refer that, when applying this procedure, the mode shapes must be normalized in such a way that their participation factor reduces to unity [25] [26]. The value of μ is to be chosen by the designer. Solving equation (5) with respect to ξ_T, one can determine the design parameters of the TMD.

The structures studied were six shear buildings with 5, 10, 15, 20, 25 and 30 stories. The plan view of each floor and the front-elevation view of the 5-stories building are presented in Figure 11, with each floor supporting a distributed load of 1 ton/m^2.
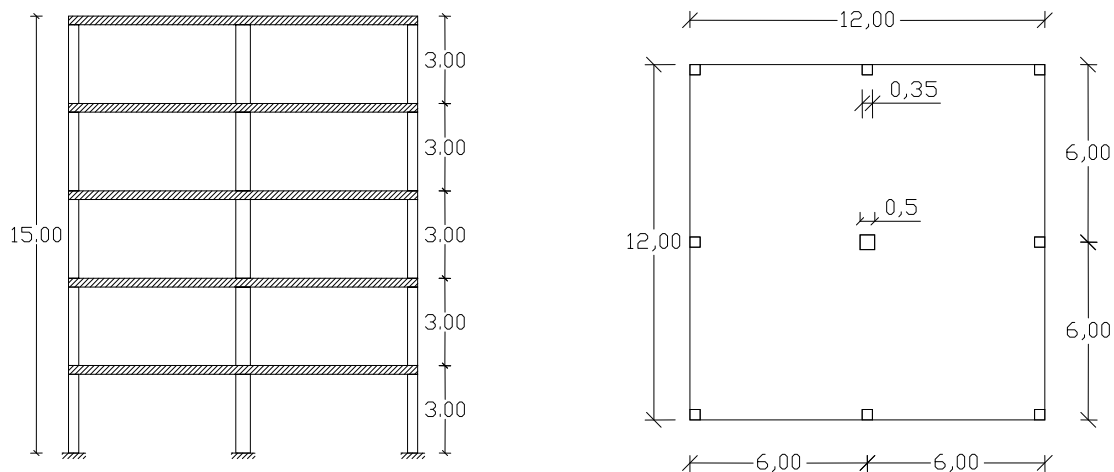

Figure 11: Plant and front-elevation views of the 5-stories building

A summary of each building geometrical, mechanical and material characteristics is given in Table 1. For all other shear buildings, the columns were considered massless and the remaining mass was considered lumped at the floor slabs. Thus, a 144 ton mass is associated with each degree of freedom (1 ton/m^2 x 12 m x 12 m).

Table 1: Geometrical, mechanical and material characteristics used in the buildings

	Columns				
	C1	C2			Slab
Cross Section	0.1225	0.25		Area	144
Inertia (m^4)	0.0012505	0.003255		m (ton/m^2)	1
E (GPa)	30			m (ton)	144
ν	0.2			ν	0.2

The first five natural frequencies of vibration for the six buildings are presented in Table 2.

Table 2: First five natural frequencies of the six buildings

Nº of Stories	Natural Frequency (Hz)				
	1	2	3	4	5
5	1.700	4.963	7.823	10.050	11.463
10	0.893	2.658	4.365	5.973	7.449
15	0.605	1.809	2.994	4.149	5.261
20	0.439	1.354	2.272	3.071	3.861
25	0.368	1.102	1.833	2.556	3.269
30	0.308	0.922	1.534	2.142	2.744

As previously mentioned, the actions considered in this study were the displacement time-histories of the 1951 El Centro and 1995 Kobe earthquakes, represented in Figures 12 and 13. The spectral content of the earthquakes is represented in Figures 14 and 15.
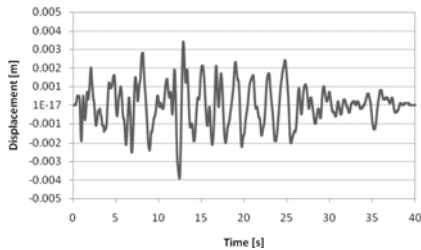

Figure 12: Displacement time-history of the 1951 El Centro earthquake
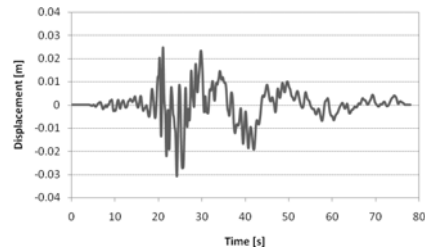

Figure 13: Displacement time-history of the 1995 Kobe earthquake
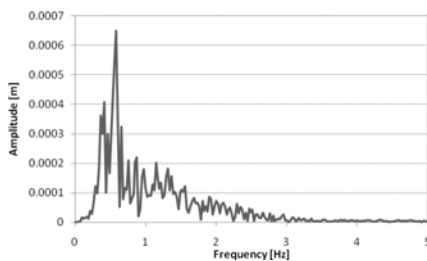

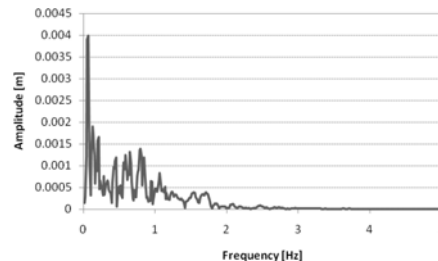Figure 14: Displacement Spectrum of the 1951 El Centro earthquake

Figure 15: Displacement Spectrum of the 1995 Kobe earthquake

In Table 3 are presented the values of the TMDs parameters as function of the mass ratio μ and the number of stories of the buildings.

Table 3: Values of the parameters of the TMDs for the six buildings

N° of Stories		μ					
		0.00	0.01	0.02	0.03	0.04	0.05
	m_T	0.0000	6.3328	12.6656	18.9984	25.3312	31.664
5	k_T	0.0000	722.5248	1445.05	2167.574	2890.099	3612.624
	c_T	0.0000	16.9336	47.8956	87.9898	135.4691	189.3239
	m_T	0.0000	12.21	24.42	36.63	48.84	61.05
10	k_T	0.0000	384.2236	768.4472	1152.671	1536.894	1921.118
	c_T	0.0000	17.3605	49.103	90.208	138.8843	194.0967
	m_T	0.0000	18.0606	36.1212	54.1817	72.2423	90.3029
15	k_T	0.0000	261.0633	522.1266	783.1899	1044.253	1305.316
	c_T	0.0000	17.4497	49.3553	90.6714	139.5978	195.0938
	m_T	0.0000	23.8184	47.6369	71.4553	95.2737	119.0921
20	k_T	0.0000	181.1357	362.2713	543.407	724.5426	905.6783
	c_T	0.0000	16.7163	47.2808	86.8604	133.7303	186.8938
	m_T	0.0000	29.7449	59.4899	89.2348	118.9798	148.7247
25	k_T	0.0000	158.9397	317.8794	476.8191	635.7588	794.6985
	c_T	0.0000	17.4982	49.4925	90.9235	139.9858	195.6362
	m_T	0.0000	35.5843	71.1686	106.7529	142.3372	177.9215
30	k_T	0.0000	132.9201	265.8402	398.7604	531.6805	664.6006
	c_T	0.0000	17.502	49.5032	90.9432	140.0162	195.6785

In Tables 4 through 9 are presented peak displacements, velocities and accelerations, corresponding to each of the 36 combinations of Table 3, for the El Centro earthquake and the Kobe earthquake, respectively.

Table 4: Peak displacements of the six buildings when subjected to the El Centro earthquake

N° of Stories	μ					
	0	0.01	0.02	0.03	0.04	0.05
5	0.0169	0.01	0.0083	0.0073	0.007	0.0067
10	0.0187	0.0157	0.0151	0.0145	0.014	0.0135
15	0.0302	0.02	0.0181	0.0169	0.016	0.0152
20	0.0275	0.0227	0.0205	0.0187	0.0171	0.0157
25	0.0314	0.0229	0.0229	0.0226	0.0222	0.0217
30	0.0257	0.0171	0.0156	0.0144	0.0138	0.0131

Table 5: Peak velocities of the six buildings when subjected to the El Centro earthquake

Nº of Stories	μ					
	0	0.01	0.02	0.03	0.04	0.05
5	0.2036	0.1026	0.0876	0.0773	0.0694	0.063
10	0.1349	0.104	0.098	0.0932	0.0889	0.0851
15	0.1858	0.086	0.0733	0.0731	0.0734	0.0729
20	0.145	0.1221	0.102	0.0849	0.0731	0.0661
25	0.1317	0.1009	0.0946	0.0878	0.087	0.0878
30	0.1286	0.104	0.0991	0.0943	0.0897	0.0853

Table 6: Peak accelerations of the six buildings when subjected to the El Centro earthquake

Nº of Stories	μ					
	0	0.01	0.02	0.03	0.04	0.05
5	2.585	1.455	1.277	1.1324	1.0146	0.9203
10	1.7743	1.0158	0.9664	0.9221	0.8789	0.8343
15	1.6478	1.031	0.8841	0.7872	0.7255	0.6885
20	0.9972	0.9514	0.8324	0.7101	0.6296	0.5892
25	1.0896	1.1133	0.9728	0.9182	0.8613	0.8239
30	1.0083	0.9196	0.7919	0.7454	0.6964	0.647

Table 7: Peak displacements of the six buildings when subjected to the Kobe earthquake

Nº of Stories	μ					
	0	0.01	0.02	0.03	0.04	0.05
5	0.2078	0.0965	0.0863	0.0796	0.0745	0.0702
10	0.1092	0.1064	0.1005	0.0949	0.0897	0.0849
15	0.2097	0.1598	0.1477	0.1394	0.1329	0.1274
20	0.137	0.1199	0.1183	0.1159	0.1132	0.1103
25	0.1198	0.1167	0.1124	0.1076	0.1027	0.0978
30	0.0938	0.0872	0.0851	0.0827	0.0801	0.0776

Table 8: Peak velocities of the six buildings when subjected to the Kobe earthquake

Nº of Stories	μ					
	0	0.01	0.02	0.03	0.04	0.05
5	2.1887	0.9267	0.8142	0.7362	0.6875	0.6475
10	0.7279	0.6725	0.6524	0.6339	0.6173	0.6019
15	0.8328	0.7188	0.6532	0.6045	0.5665	0.5357
20	0.6482	0.5635	0.5045	0.4601	0.451	0.4404
25	0.6883	0.6016	0.5819	0.5598	0.5363	0.5124
30	0.5821	0.544	0.533	0.5184	0.5016	0.4835

Table 9: Peak accelerations of the six buildings when subjected to the Kobe earthquake

Nº of Stories	μ					
	0	0.01	0.02	0.03	0.04	0.05
5	24.367	8.2491	7.4322	6.8052	6.285	5.837
10	5.8565	4.8629	4.6357	4.4125	4.2015	4.0018
15	5.4871	4.0746	3.7721	3.6174	3.5499	3.4836
20	5.0426	3.061	2.9828	2.9045	2.8173	2.7272
25	6.6715	3.7847	3.4968	3.1912	2.9796	2.7649
30	5.4031	4.0403	3.7661	3.4338	3.1303	3.0325

The results above were computed using the Newmark β-method, with a time step of 0.001s, with $\alpha=1/4$ and $\delta=1/2$ (constant average acceleration method) and with $\alpha=1/6$ and $\delta=1/2$ (linear acceleration method). The same exact results were obtained by both methods. In order to validate the results, the calculations were also performed using a numerical state-space formulation, also with a time step of 0.001s. A graphical comparison between both numerical formulations for the El Centro earthquake and for the Kobe earthquake is presented below in Figures 16-18. Such figures represent the variation of the peak displacements (respectively of the 15-20-30 storey buildings) with the TMD mass ratios for the El Centro (in black) and Kobe (in grey) earthquakes.

From the analyses of the figures, it can be seen that the response quantities are much larger when the buildings are subjected to the Kobe earthquake than when they are subjected to the El Centro earthquake. The natural frequencies resulting of the application of a TMD to the 15-20-30-stories buildings are summarized in Tables 10, 11 and 12.

Table 10: Frequencies resulting from the application of a TMD to control the first mode of vibration of the 15-stories building

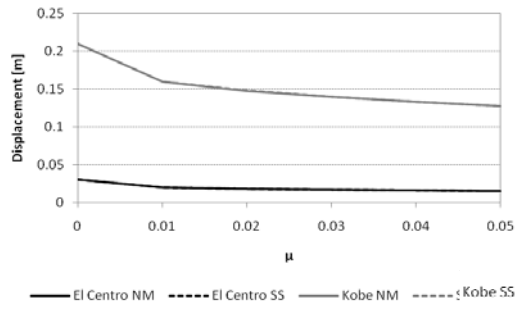|	μ				
	0.01	0.02	0.03	0.04	0.05
f1 (Hz)	0.5674	0.5523	0.5409	0.5315	0.5233
f2 (Hz)	0.6442	0.6607	0.6734	0.6842	0.6937

Figure 16: Peak displacements of the 15-storey building when subjected to El Centro and Kobe earthquakes
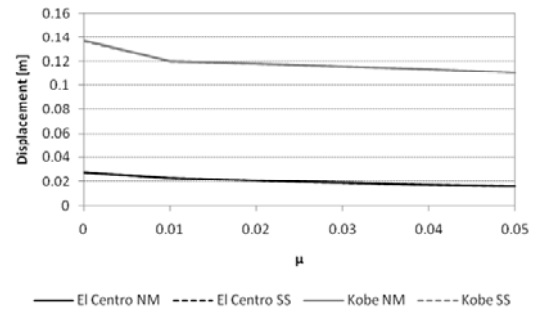

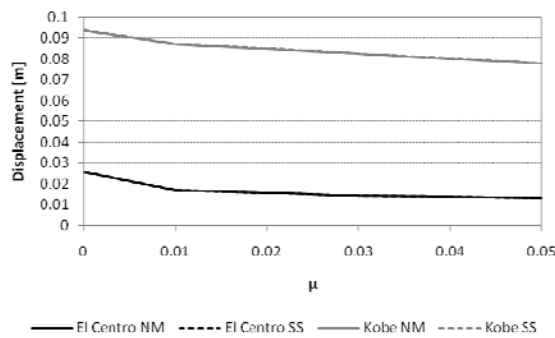Figure 17: Peak displacements of the 20-storey building when subjected to El Centro and Kobe earthquakes

Figure 18: Peak displacements of the 30-storey building when subjected to El Centro and Kobe earthquakes

Table 11: Frequencies resulting from the application of a TMD to control the first mode of vibration of the 20-stories building

	μ				
	0.01	0.02	0.03	0.04	0.05
f1 (Hz)	0.4126	0.4021	0.3941	0.3875	0.3818
f2 (Hz)	0.4661	0.4776	0.4864	0.4939	0.5006

Table 12: Frequencies resulting from the application of a TMD to control the first mode of vibrationof the 30-stories building

	μ				
	0.01	0.02	0.03	0.04	0.05
f1 (Hz)	0.2884	0.2807	0.2749	0.2701	0.2659
f2 (Hz)	0.3275	0.3358	0.3423	0.3478	0.3526

TMD Application to a Bridge at Porto

The bridge whose dynamic behaviour was studied in this paper was based on a steel pedestrian bridge located in the city of Porto, Portugal. It connects a shopping centre with the City Park. This bridge presented high levels of vertical vibration when cross by a single pedestrian, a very uncomfortable situation for the users.

The bridge has two spans, each with 30m in length, in horizontal projection, with 6% slope. The higher end of the bridge is supported on the shopping centre and the lower end rests on a footpath of the park. A reinforced concrete column provides the support of the middle section. A side view of the bridge is presented in Figure 19.
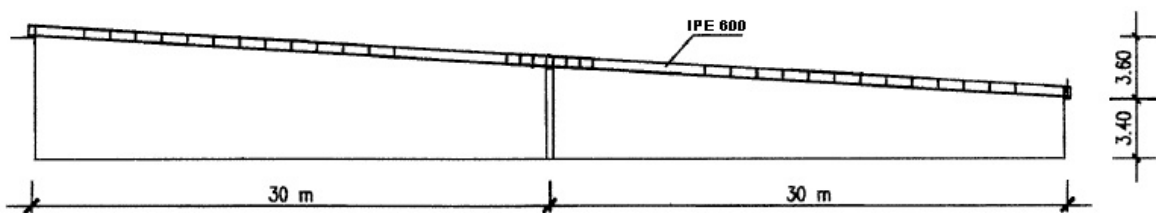
Figure 19 – Side view of the bridge

The bridge is materialized by two IPE 600 beams place side by side about 3.5m apart. These metallic profiles are joined together by HEB 100 profiles spaced 1.5m, placed perpendicularly to the IPE 600 beams. The pavement of the bridge is supported by diagonals constituted by T 40 profiles. A top view of the bridge is presented in Figure 20.
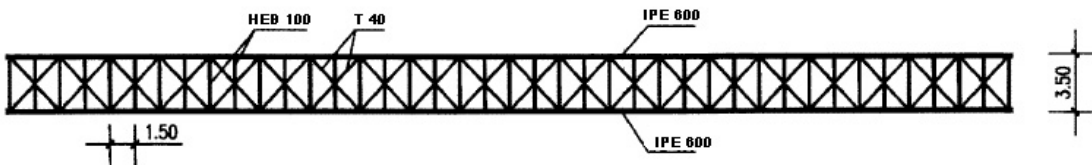
Figure 20 – Top view of the bridge

A summary of the bridge's characteristics is presented in Table 13.

Table 13 – Geometrical, mechanical and material characteristics of the bridge

Cross Section (m^2)	Inertia (m^4)	E (GPa)	ν	m (kg/m)
0.0312	0.0018416	200	0.3	425.78

Based on the geometrical and mechanical characteristics of the bridge, a simple finite element model of it was developed in order to determine some of its dynamical characteristics. Since only its vertical flexional behavior was of importance to the study, the finite element model was constructed considering a single equivalent beam with the properties presented in Table 13. The modal parameters of the first four modes of vibration are given in Table 14.

Table 14 – Modal parameters of the first four modes of vibration

Mode	f_{Sj} (Hz)	ω_{Sj} (rad/s)	M_{Sj} (Ton)	K_{Sj} (kN/m)	ξ_{Sj}
1	1.617	10.160	12.801	1322.3	0.0128
2	2.527	15.878	11.268	2840.7	0.0128
3	6.469	40.646	12.939	21376.9	0.0219
4	8.187	51.440	11.246	29757	0.0268

where f_{Sj} is the natural frequency of vibration of the jth mode, in Hz, ω_{Sj} is the natural frequency of vibration of the jth mode, in rad/s, M_{Sj} is the modal mass of the jth mode, K_{Sj} is modal stiffness of the jth mode and ξ_{Sj} is the damping ratio of the jth mode.

The graphical configurations of the first four modes of vibration are shown in Figure 21.

1st mode

2nd mode

3rd mode

4th mode
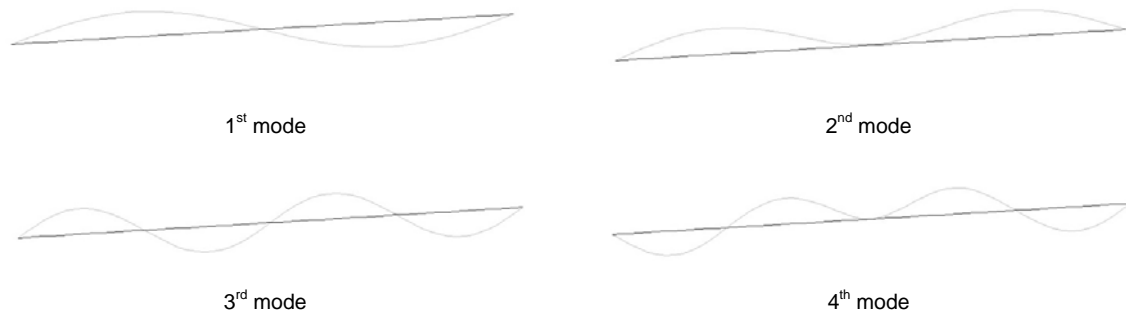
Figure 21 – Configuration of the first four modes of vibration of the bridge

When studying the dynamical behaviour of the bridge, only the comfort of its users was of interest. In this way, only the actions induced by the crossing of the bridge by pedestrians were considered. After analysing the natural frequencies of the bridge, it was noticed that its first two natural frequencies coincided with the frequency of two types of pedestrian motion:

- The first frequency, 1.617Hz, is approximately the frequency of a person walking in a somewhat slow motion

- The second frequency, 2.527Hz, is approximately the frequency of a person practicing jogging

Thus, these were the actions that this study took into account. The modelling of the actions considered that the bridge was crossed by a single pedestrian with 65kg of mass, with stepping frequencies of 1.617Hz and 2.527Hz. Graphical representations of the load functions of a walking pedestrian and of a jogging pedestrian are presented in Figures 22 and 23. Their theoretical formulations are detailed by Paredes [27].

After simulating the effects of a pedestrian walking and jogging across the bridge on the finite element model, the values of the acceleration time history for each situation were obtained.
Since walking only excites the first mode of vibration and jogging only excites the second mode of vibration, the maximum values of acceleration will occur at the points that present the absolute maximum modal amplitude. In the first mode, those points are located at 15m and 45m, with equal amplitude but with opposite sign. In the second mode those points are located at 13m and 47m, with equal amplitude and sign.
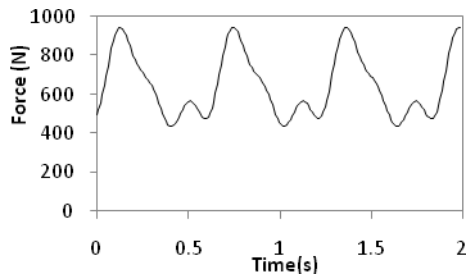
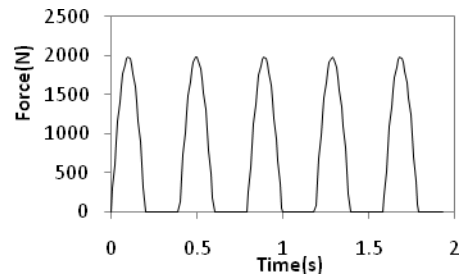Figure 22 – Load function of a 65kg pedestrian walking with a frequency of 1.617Hz

Figure 23 – Load function of a 65kg pedestrian running with a frequency of 2.527Hz

After simulating the effects of a pedestrian walking and jogging across the bridge on the finite element model, the values of the acceleration time history for each situation were obtained. Since walking only excites the first mode of vibration and jogging only excites the second mode of vibration, the maximum values of acceleration will occur at the points that present the absolute maximum modal amplitude. In the first mode, those points are located at 15m and 45m, with equal amplitude but with opposite sign. In the second mode those points are located at 13m and 47m, with equal amplitude and sign.

Table 15 presents the peak values of the acceleration as function of the stepping frequency and of the position along the bridge. Figures 24-27 present the graphical representation of the acceleration time history for the crossing of the bridge.

Table 15 – Peak accelerations of the bridge before the application of the TMD

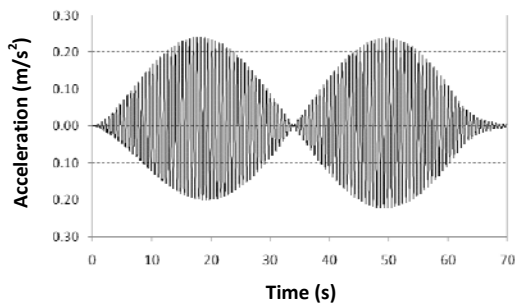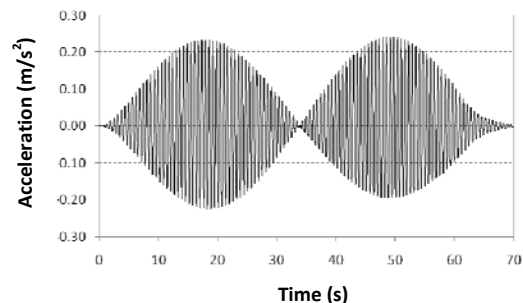| f_S (Hz)	x (m)	Acceleration (m/s^2)
1.617	15	0.240
	45	0.241
2.517	13	0.905
	47	0.891

Figure 24 – Accelerations measured at x=15m for walking frequency of 1.617Hz, before the application of the TMD

Figure 25 – Accelerations measured at x=45m for walking frequency of 1.617Hz, before the application of the TMD
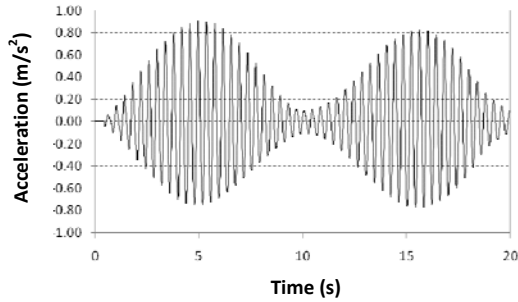
16

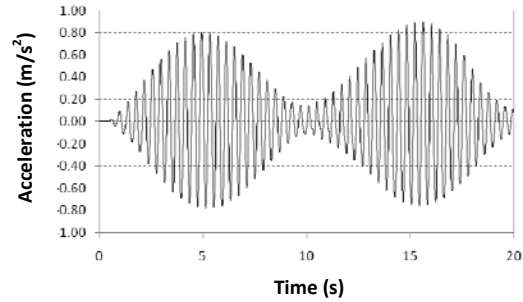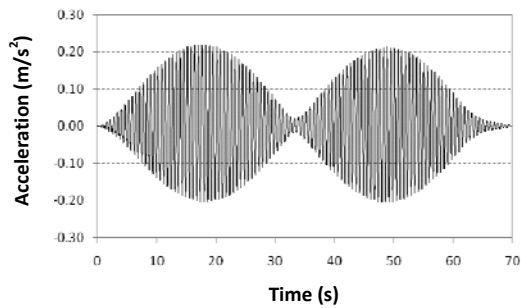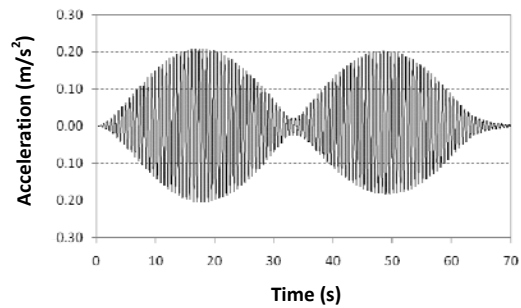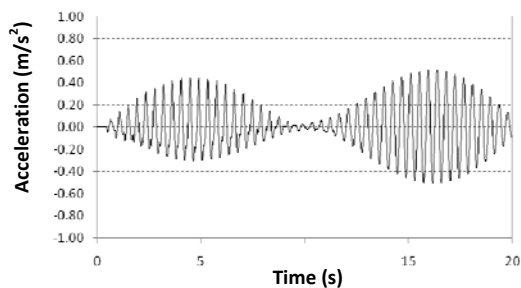Figure 26 – Accelerations measured at x=13m for running frequency of 2.527Hz, before the application of the TMD

Figure 27 – Accelerations measured at x=47m for running frequency of 2.527Hz, before the application of the TMD

According to the british standard BS 5400, the maximum vertical acceleration of this bridge should not exceed $0.63m/s^2$. Since this value is surpassed when the bridge is crossed by a running pedestrian, it is justified the study of the application of a TMD to control the excessive vibration levels of the second mode.

The detailed design procedure of the TMD was presented by Paredes [27]. A summary of its optimum design parameters is presented in Table 16.

Table 16 – Design parameters of the TMD

m_T	k_T	c_T	μ	q	ξ_T
225.36kg	53731.17N/m	585.08kg/s	0.02	0.9725	0.05

where m_T is mass of the TMD, k_T is the stiffness of the TMD, c_T is damping constant of the TMD, μ is mass ratio of the TMD the modal mass of the second mode of vibration, q is the ratio of the TMD frequency to frequency of the second mode of vibration and ξ_T is the damping ratio of the TMD.

The simulation of the implementation of the TMD in the finite element model suppressed the second mode of vibration and gave birth to two new modes of vibration. The first had a natural frequency of 2.343Hz and the second had a natural frequency of 2.688Hz. The first mode of vibration of the bridge remained unchanged, with a natural frequency of vibration of 1.617Hz.

To check the efficiency of the TMD, a new analysis was performed. To do so, the simulation of pedestrian running across the bridge with stepping frequencies of 2.343Hz and 2.688Hz, the frequencies of the new modes of vibration.

Table 17 presents the peak values of the acceleration as function of the stepping frequency and of the position along the bridge, after the implementation of the TMD. Figures 28-33 present the graphical representation of the acceleration time history for the crossing of the bridge.

17

Table 17 – Peak accelerations of the bridge after the application

f_S (Hz)	x (m)	w/o TMD	w/ TMD	Reduction
1.617	15	0.240	0.219	6.5%
	45	0.241	0.208	13.7%
2.343	13	0.905	0.515	43.1%
	47	0.891	0.662	25.7%
2.688	13	0.905	0.560	38.1%
	47	0.891	0.527	40.9%

Figure 28 – Accelerations measured at x=15m for walking frequency of 1.617Hz, after the application of the TMD

Figure 29 – Accelerations measured at x=45m for walking frequency of 1.617Hz, after the application of the TMD

Figure 30 – Accelerations measured at x=13m for running frequency of 2.343Hz, after the application of the TMD
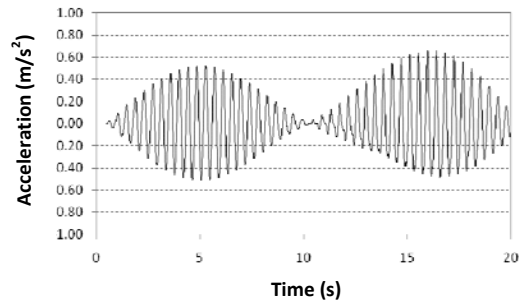

Figure 31 – Accelerations measured at x=47m for running frequency of 2.343Hz, after the application of the TMD
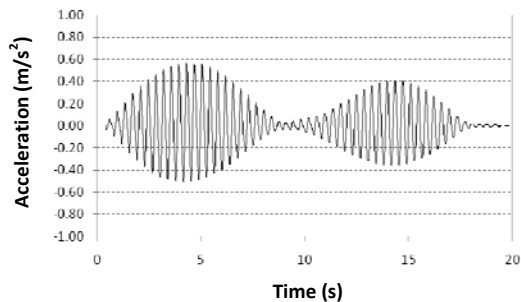

Figure 32 – Accelerations measured at x=13m for running frequency of 2.688Hz, after the application of the TMD
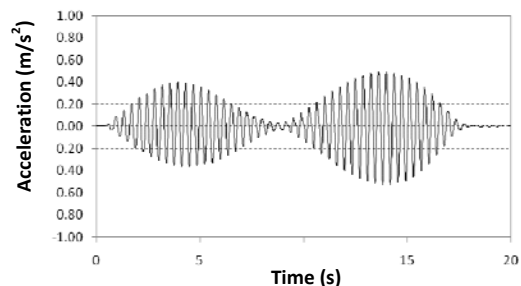

Figure 33 – Accelerations measured at x=47m for running frequency of 2.688Hz, after the application of the TMD

As can be seen from the observation of Table 17, the maximum acceleration measured on the bridge is $0.662m/s^2$, which is superior to established limit of $0.63m/s^2$. However, since this limit is only surpassed by 5%, a reasonable error in what civil engineering is concerned and since one is dealing with comfort criteria and not safety criteria, the design of the TMD can be considered acceptable.

SEMI-ACTIVE AND HYBRID CONTROL OF STRUCTURAL VIBRATIONS

Semi-Active Control

The next step is to use semi-active devices to control the vibration of a base excited structure. Among the possible semi-active technologies, the magneto-rheological fluid based devices are seen as a promising solution for structural control.

Basically two types of rheological fluids can be used to create a structural control system: Magneto-rheological (MR) and Electro-rheological (ER) fluids. MR fluids are materials that exhibit a change in rheological properties with the application of a magnetic field while ER fluids exhibit rheological changes when an electric field is applied to the fluid.

Although power requirements are approximately the same MR fluids only require small voltages and currents while ER fluids require very large voltages and very small currents. However, ER fluids have many disadvantages including relatively small rheological changes and significant property changes with temperature. Thus, MR fluids have become an extensively studied "smart" fluid and some experimental research has been done in the last years to produce a "smart" control device with this fluid.

Usually, the MR fluid devices are built to operate in the following modes (Figure 34): valve mode or flow mode; direct shear mode or clutch mode; squeeze film compression mode and the combination of some of the previous modes.
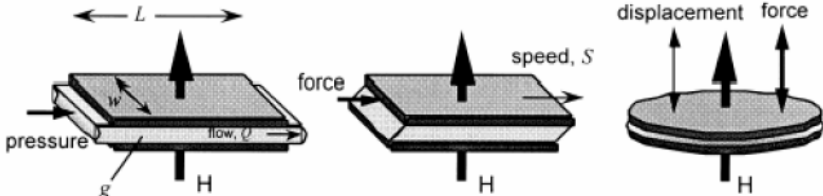

Figure 34: Basic operation modes of MR-fluid.

For vibration control purposes the "smart" MR fluid effect is interesting since it is possible to apply this phenomenon to create a variable damping device or a "smart" hydraulic damper. The current applied to a MR fluid essentially allows controlling the damping force without the need of mechanical valves that are commonly used in adjustable dampers. This offers the possibility to create a reliable damper since a failure in the control system reverts the MR damper to a passive damper (Figure 35).
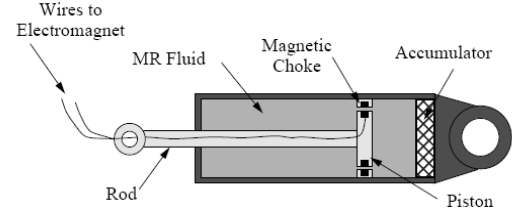

Figure 35: Schematic representation of a magneto-rheological damper.

19

The MR damper performance is often characterized by using the force vs. velocity relationship. Regular viscous damper has an ideal linear constitutive behaviour and the slope of the line is known as the damper coefficient. In the case of MR dampers the possibility to change the damping characteristics leads to a force vs. velocity envelope that can be described as an area rather than a line in the force-velocity plane. This behaviour is the fundamental condition to build a "smart" damper since it is possible to design a controller to follow any force-velocity relationship within the envelope to create a control strategy.

According to the available bibliography two common methods can be used to model MR devices such as MR dampers: the parametric modelling technique that characterizes the device as a collection of springs, dampers, and other physical elements; the non-parametric modelling that employ analytical expressions to describe the characteristics of the modelled devices. Many authors have developed modelling techniques for the MR dampers based on both methods. In recent studies Dyke *et al* [28] presented a simple parametric model based on the extension of the Bouc-Wen model that allows a good approximation to the real MR damper behaviour as shown in Figure 36.
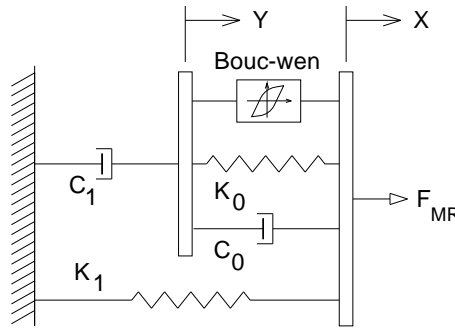

Figure 36: Modified Bouc-Wen model for a MR damper.

The Bouc-Wen model is based on the Markov-vector formulation to model nonlinear hysteretic systems and according with the modified model shown in Figure 36, the MR force can be computed by

$$F_{MR} = c_1 \dot{y} + k_1 \left(x - x_0 \right) \tag{6}$$

$$\begin{cases} \dot{y} = \dfrac{1}{\left(c_0 + c_1 \right)} \left\{ \alpha z + c_0 \dot{x} + k_0 \left(x - y \right) \right\} \\ \dot{z} = -\gamma \left| \dot{x} - \dot{y} \right| z \left| z \right|^{n-1} - \beta \left(\dot{x} - \dot{y} \right) \left| z \right|^{n} + A \left(\dot{x} - \dot{y} \right) \end{cases} \tag{7}$$

In these equations z is the revolutionary variable, F_{MR} is the predicted damping force, k_1 is the accumulator stiffness, c_0 is the viscous damping observed at larger velocities and the parameters β, γ and A allows controlling the linearity in the unloading and the smoothness of the transition from the pre-yield to the post-yield region. The dashpot c_1 is included to produce the roll-off at low velocities, k_0 is used to control the stiffness at larger velocities, and x_0 is the initial displacement of spring k_1 associated with the nominal damper due to the accumulator.

$$\begin{cases} c_1 = c_{1a} + c_{1b}u \\ c_0 = c_{0a} + c_{0b}u \\ \alpha = \alpha_a + \alpha_b u \\ u = -\eta(u-v) \end{cases} \qquad (8)$$

The damping constants c_0 and c_1 depend on the electrical current applied to the MR damper. The variable u is the current applied to the damper through a voltage-to-current converter with a time constant η and the variable v is the voltage applied to the converter.

A simple MATLAB/SIMULINK block diagram can be used to simulate the Bouc-Wen model of a MR damper as shown in Figure 37.
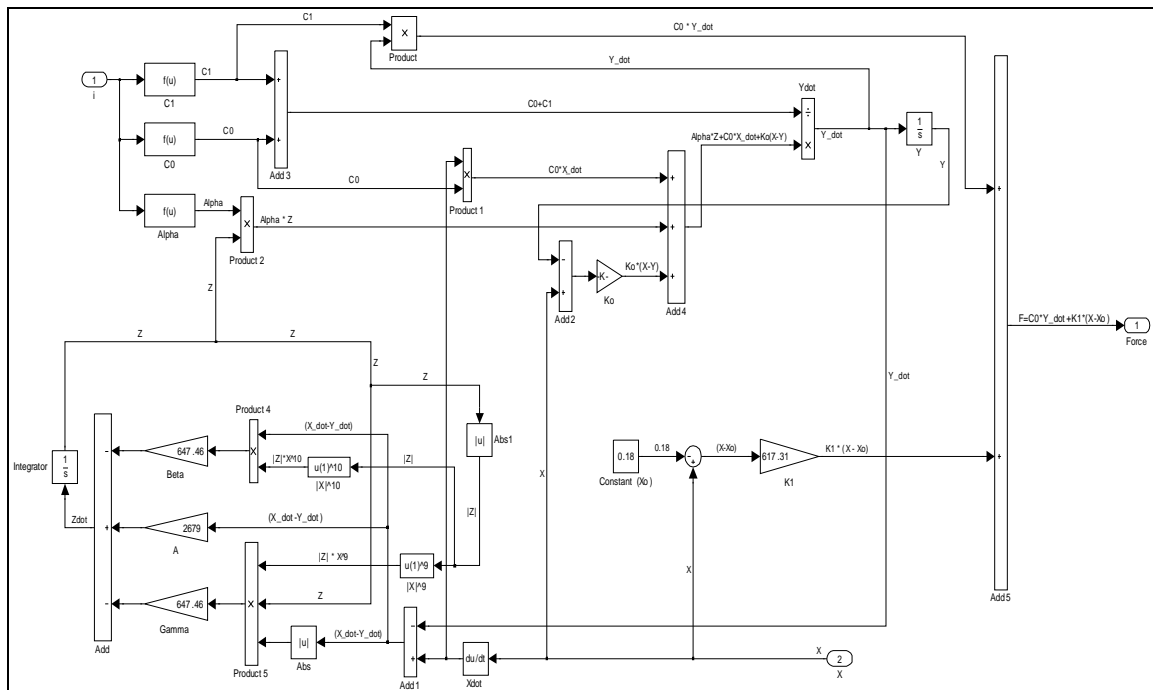

Figure 37: Block diagram of a Magneto-rheological damper using a Bouc-Wen model.

To study the behaviour of a MR damper some experiments were carried out on a MTS universal testing machine, of the Mechanical Engineering Laboratory at FEUP, with the MR damper device RD-1005-3 supplied by LORD Corporation (Figure 38). According to the device specifications it has a capacity to provide a peak to peak force of 2224 N at a velocity of 51 mm/s with a continuous current supply of 1 A. The MR damper was tested using the computer-controlled servo hydraulic MTS universal testing machine shown in Figure 39. The MR damper was attached to the MTS machine (operating under displacement control mode) and a 5 kN load cell was incorporated at the upper head to measure the force applied to the damper. The results were automatically collected by the computer-controlled MTS equipment and stored in a desktop PC.
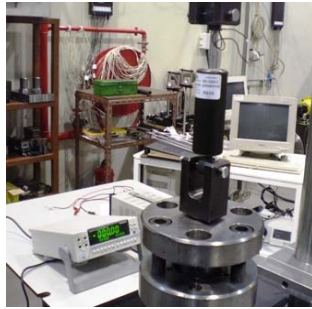
Parameter	Value
Extended length	208mm
Device stroke	±25mm
Max. Tensile force	4448N
Max. temperature	71ºC
Compressed length	155mm
Response time	<10ms
Max. Current supply	2A

Figure 38: Magneto-rheological damper RD-1005-03 test setup at FEUP.

Figure 39: Magneto-rheological damper with current supply device, connected to MTS universal setup (FEUP).

After assemblage, the MR damper was forced with a sinusoidal signal at a fixed frequency, amplitude and current supply. To obtain the response of the MR damper under several combinations of frequencies, amplitudes and current supplies a series of tests were carried out. Therefore, a set of frequencies (0.5, 1.0, 1.5 and 2.0 Hz), amplitudes (2, 4, 6, 8 and 10 mm) and current supplies (0.0, 0.1, 0.2, 0.25, 0.5, 0.75, 1.0 and 1.5 A) were used to complete the test program. In order to control and avoid temperature failure, especially at higher frequencies, a thermocouple was used to measure the external temperature of the MR damper. Typical results of this experimental research are shown in Figures 40 and 41.
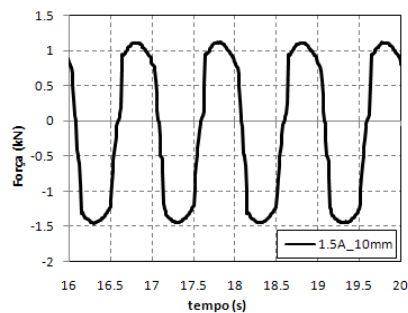

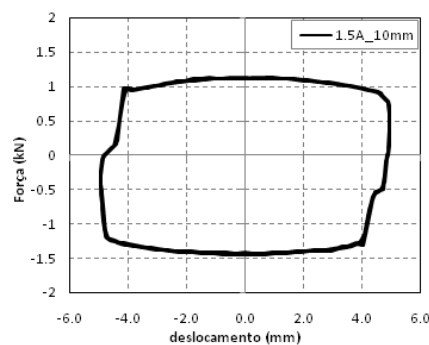Figure 40: MR damper RD-1005-03 Force-Time History (1.5 A and 10mm).

Figure 41: MR damper RD-1005-03 Force-Displacement curves (1.5 A and 10mm).

22

The variable current tests demonstrate that increasing the input current implies an increase in the force required to yield the MR fluid and a plastic-like behaviour in observed in the hysteretic loop. In the frequency dependent test is observed that the maximum damping force increases with the frequency due to large plastic viscous force at higher velocity.

According with the scheduled research program the next step will be to study the experimental dynamic behaviour of a scaled metallic load frame with passive and semi-active devices, namely MR dampers (Figure 42). This frame will be tested at the FEUP-Covicocepad Lab using the QUANSER shaking table II shown in Figure 43.

The experimental research employs three control strategies: (1) a passive control based on base isolation devices; (2) a semi-active control based on a MR damper assembled to the structure; (3) a hybrid control technique through the association of the base isolation devices with the MR damper.

To study the semi-active control strategy a MR damper is placed at the first floor level attached to the frame and rigidly attached to the shaking table. The structure is excited using the N-S component of the 1940 El Centro earthquake as the seismic ground acceleration, time-scaled with Froude similarity according to the shaking table model, in order to obtain the frequency characteristics of the structure and the physical model parameters.
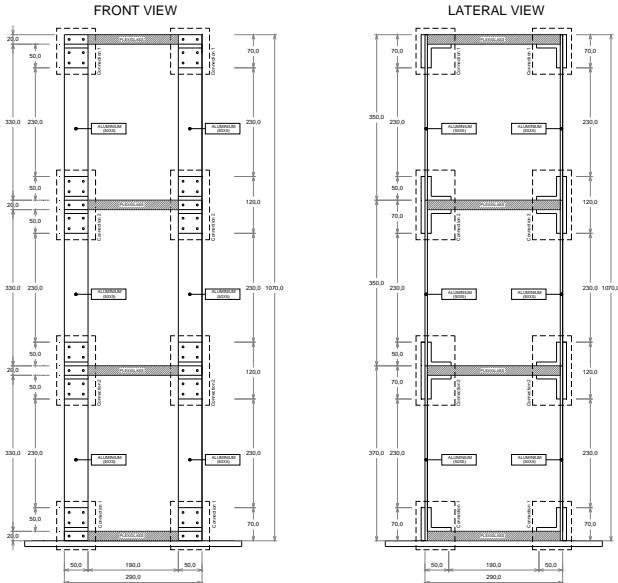

Figure 42: 3-DOF small metallic frame at FEUP – Covicocepad Lab.

Figure 43: Quanser shaking table II (and its controllers) at FEUP – Covicocepad Lab.

The equation of motion that describes the behaviour of a controlled building under an earthquake load is given by:

$$M\ddot{x} + C\dot{x} + Kx = -\Gamma f - M\lambda\ddot{x}_g \qquad (9)$$

where M is the mass matrix, C is the damping matrix, K is the stiffness matrix, x is the vector of floors displacements, $\dot{x}$ and $\ddot{x}$ are the floor velocity and the acceleration vectors respectively, f is the measured control force, λ is a vector of ones and Γ is a vector that accounts for the position of the MR damper in the structure.

This equation can be rewritten in the state-space form as

$$\dot{z} = Az + Bf + E\ddot{x}_g \qquad (10)$$

$$y = Cz + Df + v \qquad (11)$$

where z is the state vector, y is the vector of measured outputs and v is the measurement noise vector. The other variables are defined by

$$A = \begin{bmatrix} 0 & I \\ -M^{-1}K & -M^{-1}C \end{bmatrix} \qquad B = \begin{bmatrix} 0 \\ M^{-1}\Gamma \end{bmatrix} \qquad E = -\begin{bmatrix} 0 \\ \lambda \end{bmatrix}$$

$$C = \begin{bmatrix} -M^{-1}K & -M^{-1}C \\ I & 0 \end{bmatrix} \qquad D = \begin{bmatrix} M^{-1}\Gamma \\ 0 \end{bmatrix} \qquad (12)$$

To control this semi-active structure based on a control force determination, usually are measured: the absolute acceleration of some relevant selected points in the structure; the displacement of the control device; and the control force.

Control algorithms

After calibrating the MR damper numerical model it is necessary to select a proper control algorithm to efficiently use this device in reducing the dynamic response of structural systems. Obviously, the control strategy depends on the MR damper model selected to simulate the nonlinear hysteretic behaviour of this device (Jansen and Dyke [29], Kang-Min *et al* [30]).

The fundamental condition to operate the MR damper is based on a generated damping force that is related with the input voltage; the control strategy is selected so that the damping force can track a desired command damping force. The available models can be categorized in static and dynamic models. The basic difference between them is that the static models do not include dynamic relation between input and output.

As mentioned before this work is based on the Bouc-Wen model that can represent the hysteresis dynamics explicitly. Therefore, an efficient control algorithm must be developed or chosen from the available research bibliography to correctly characterize the intrinsic MR fluid behaviour, maximizing the MR damper characteristics as a semi-active control device.

In the last few years several approaches have been proposed and intensively studied for better selection of the input voltage that must be applied to the MR damper to achieve the maximum performance. Among the proposed strategies the following are the most studied: Lyapunov Based Control; Decentralized Bang-Bang Control; LQG (Linear Quadratic Gaussian) or Clipped-Optimal Control; H$_2$/LQG control; Fuzzy Control and also Artificial Neural Network (ANN) control strategies. Some of these control strategies will be applied in this research program in order to understand the pros and cons of each strategy. After performing an exhaustive study on the numerical model and small mock-up experimental model, the more reliable vibration control algorithms will be applied to medium-scale experimental models.

Clipped-Optimal Control

A semi-active clipped-optimal control based on acceleration feedback was proposed by Dyke *et al*. [28]. The control diagram of this control strategy is shown in Figure 44.
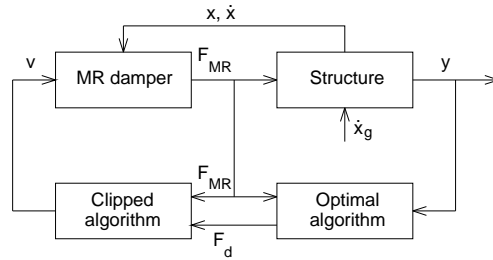

Figure 44: Semi-active clipped-optimal control diagram.

As shown in the diagram this strategy has two controllers and is based on a linear optimal controller designed to set the command signal to zero or to the maximum level. The signal is selected according with the desired command force, and the comparison between this force and the effective MR damper force. In this case, the command signal can be computed as

$$F_{MR} = \begin{cases} F_d, & F_d \cdot \dot{x}_{dev} < 0 \\ 0, & otherwise \end{cases}$$

(13)

where F_{MR} is the control force of the MR damper and $\dot{x}$ is the velocity across the damper.

Fuzzy Control

One of the recent semi-active control strategies is based on the fuzzy control inference. As shown in Figure 45, this strategy has only one controller.
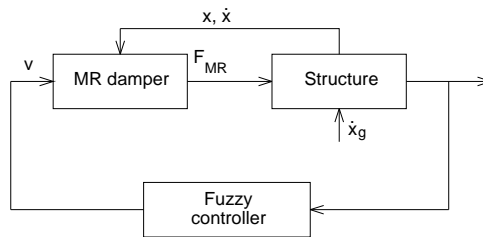

Figure 45: Semi-active clipped-optimal control diagram.

The fuzzy algorithm is used to compute the command signal and the voltage is selected using a fuzzy rule inference. The model can much easier accommodate uncertainties of input data and structural response sensors. Also is a more reliable strategy since is fail-safe since it guarantees the bounded-input/ bounded-output stability of the controlled structure [30].

CONCLUSIONS

Some R&D done recently within COVICOCEPAD project, approved in the framework of Eurocores program, was described. Some applications/results with a few control devices/techniques for control of structural vibrations were outlined, using namely: base isolation, TLD's and MR dampers. Applications of TMD's devices to two civil engineering structures under dynamic and seismic actions were also described.

ACKNOWLEDGEMENTS

REFERENCES

[1] R.C. Barros, P. Belli, I. Corbi and M. Nicoletti; "Large Scale Risk Prevention", *International Journal of Earthquake Engineering and Engineering Seismology*, European Earthquake Engineering 1.04, ISSN 0394-5103, Vol. XVIII, No.1, pp. 10-19, Patròn Editore, Bologna, Italy 2004.

[2] R.C. Barros, R. Bairrão, F. Branco, I. Corbi, M. Kemppinen, G. Magonette, F. Paulet and G. Serino; "Implementation of Structural Control", *International Journal of Earthquake Engineering and Engineering Seismology*, European Earthquake Engineering 2.05, ISSN 0394-5103, Vol. XIX, No.2, pp. 51-68, Patròn Editore, Bologna, Italy 2005.

[3] R.C. Barros, "Seismic Response of Tanks and Vibration Control of their Pipelines", *Journal of Vibroengineering*, Vol. 4, 2002 - No. 1 (8), Index 136, pp. 9-16, Proceedings Research Center of the Public Institution Vibromechanika, Vilnius, Lithuania, 2002.

[4] R.C. Barros, "Project COVICOCEPAD under Smart Structural Systems Technologies of Program Eurocores"; World Forum on Smart Materials and Smart Structures Technologies (SMSST-2007) Chonqing and Nanjing (China), 22-27 May 2007; in: *Smart Materials and Smart Structures Technology*; Editors: M. Tomizuka, B.F. Spencer, C.B. Yun, W. Chen, R. Chen; Taylor & Francis Ltd, 2008.

[5] R.C. Barros and O. Corbi, "Computational and Experimental Developments of Vibration Control using Liquid Tanks for Energy Dissipation Purposes in Civil Engineering Structures", Proceedings of ECCOMAS Thematic Conference "*Computational Methods in Structural Dynamics and Earthquake Engineering* (COMPDYN 2007)", Ed.: M. Papadrakakis, D.C. Charmpis, N.D. Lagaros, V. Tsompanakis; Rethymno, Creta (Greece), 13-16 June 2007, Book of Abstracts pp. 268, Full paper 1732 - 13 pages, 2007.

[6] Rui Carneiro de Barros and Ottavia Corbi, "An Overview on Some Ongoing Computational and Experimental Campaigns on Vibration Control by Liquid Tanks", *International Journal of Mechanics and Solids*, ISSN 0973-1881, Volume 3, Number 1, pp. 1-22, Research India Publications, India, 2008.

[7] L. Guerreiro, R.C. Barros and R. Bairrão; "Algorithms for Semi-Active Devices Control", Proceedings of ECCOMAS Thematic Conference "*Computational Methods in Structural Dynamics and Earthquake Engineering* (COMPDYN 2007)", Ed.: M. Papadrakakis, D.C. Charmpis, N.D. Lagaros, V. Tsompanakis; Rethymno, Creta (Greece), 13-16 June 2007, Book of Abstracts pp. 262, Full paper 1733 – 6 pages, 2007.

[8] R. Bairrão, R.C. Barros and L. Guerreiro; "Shaking Table Tests in the Aim of Project COVICOCEPAD" (Comparison of Vibration Control in Civil Engineering Using Passive and Active Dampers), Proceedings of ECCOMAS Thematic Conference "*Computational Methods in Structural Dynamics and Earthquake Engineering* (COMPDYN 2007)", Ed.: M. Papadrakakis, D.C. Charmpis, N.D. Lagaros, V. Tsompanakis; Rethymno, Creta (Greece), 13-16 June 2007, Book of Abstracts pp. 260, Full paper 1731 – 5 pages, 2007.

[9] C.F. Oliveira, R. Bairrão, R.C. Barros and L. Guerreiro; "The New Generation of Seismic Semi-Active and Active Protection Systems"; *4th European Conference on Structural Control* (4ECSC), Paper 227, St Petersbourg, Russia, 8-12 September 2008.

[10] R. Bairrão, L. Guerreiro and R.C. Barros; "Shaking Table Tests on Semi-Active Tuned Mass and Tuned Liquid Dampers"; *14 WCEE*, Beijing, China, 12-17 October 2008.

[11] A. Baratta, I. Corbi and O. Corbi; "On the Dynamics of Unilaterally Supported Rigid Blocks", *14 WCEE*, Beijing, China, 12-17 October 2008.

[12] R.C. Barros, A. Baratta, O. Corbi, et al.; "R&D on control of vibrations under COVICOCEPAD during 2007-2008", *Computational Methods in Structural Dynamics and Earthquake Engineering* (COMPDYN 2009), M. Papadrakakis, N.D. Lagaros, M. Fragiadakis (eds.), Rhodes, Greece, 22–24 June 2009 (*in press*).

[13] M.M. Paredes, R.C. Barros and A.F. Cunha; "A Parametric Study of TMD's for Regular Buildings under Earthquakes", *Computational Methods in Structural Dynamics and Earthquake Engineering* (COMPDYN 2009), M. Papadrakakis, N.D. Lagaros, M. Fragiadakis (eds.), Rhodes, Greece, 22–24 June 2009 (*in press*).

[14] F. Naeim and J.M. Kelly, *Design of Seismic Isolated Structures*: from Theory to Practice, John Wiley & Sons Inc., New York - USA, 1999.

[15] T.T. Soong and G.F. Dargush, *Passive Energy Dissipation Systems in Structural Engineering*, John Wiley & Sons Ltd, Chichester - England, 1999.

[16] R.C. Barros and M.B. César, "Seismic Behaviour of an Asymmetric Three-Dimensional Steel Frame with Base Isolation Devices"; in: *Computational Structures Technology*; Editors: B.H.V. Topping, G. Montero and R. Montenegro; Paper 252, Civil-Comp Press, Stirlingshire, Scotland, 2006.

[17] M.B. César and R.C. Barros, "Influence of Resistant Cores Location on the Seismic Response of a R/C 3D-Frame Equipped with HDRB Base Isolation Devices"; in: *Civil Engineering Computing*; Editor: B.H.V. Topping; Paper 199, Civil-Comp Press, Stirlingshire, Scotland, 2007.

[18] E. Figueiredo and R.C. Barros, "An Insight on the Influence of Damping in Seismic Isolation", in: *Civil Engineering Computing*, Editor: B.H.V. Topping, Civil-Comp Press, Paper 201, Civil-Comp Press, Stirlingshire, Scotland, 2007.

[19] A. Baratta and I. Corbi, "On the optimal design of structural base isolation devices"; in: *Computational Mechanics*: 283-285; Edts: E. Lund, N. Olhoff, J. Stegmann; Aalborg University, Denmark, 2002.

[20] A. Baratta and I. Corbi, "Optimal design of base-isolators in multi-storey buildings". *Int. J. Computers & Structures*, vol. 82, Issues 23-26: 2199-2209, Elsevier, 2004.

[21] A. Kareem, "Next Generation of Tuned Liquid Dampers", *Proc. First World Conf. on Structural Control*, Vol. 3 : pp. 19-28, International Association for Structural Control, Los Angeles, 1994.

[22] O. Corbi, "Experimental Investigation on Sloshing Water Dampers Attached to Rigid Blocks", *Proc. 5th Wseas Int. Conf. Applied Comp. Science*, Hangzhou, China, 2006.

[23] R.C. Barros, *Seismic Analysis and Design of Bottom Supported Anchored Metallic Tanks*, Edições INEGI - Instituto Engenharia Mecânica e Gestão Industrial, ISBN: 978-972-8826-18-5, FEUP, Porto, Portugal, 2008.

[24] R. Villaverde, "Reduction in Seismic Response with Heavily-Damped Vibration Absorbers". *Earthquake Engineering and Structural Dynamics*, Vol. 13, 33-42, John Wiley & Sons, Chichester, 1985.

[25] R. W Clough and J. Penzien, *Dynamics of Structures*, 3rd Edition, Computers & Structures Inc, 1995.

[26] A.K. Chopra, *Dynamics of Structures – Theory and Application to Earthquake Engineering*, 3rd Edition, Pearson-Prentice Hall, 2007.

[27] Paredes, M.. M., *Use of TMDs in Structural Vibration Control: application to bridges and to framed buildings*). M..Sc. thesis in structural engineering, FEUP, Porto, Portugal, July 2008 (in Portuguese).

[28] S.J. Dyke, B. F. Spencer, M.K. Sain, and J.D. Carlson; "Modeling and control of magnetorheological dampers for seismic response reduction", *Smart Materials and Structures*, Vol. 5, pp. 565-575, 1996.

[29] L.M. Jansen and S.J. Dyke, "Semi-active control strategies for MR dampers: A comparative study", *ASCE Journal of Engineering Mechanics*, Vol. 126, No. 8, pp. 795-803, 1999.

[30] C. Kang-Min, C. Sang-Won, J. Hyung-Jo and L. In-Won; "Semi-active fuzzy control for seismic response reduction using magnetorheological dampers", *Earthquake Engineering and Structural Dynamics*, Vol. 33, pp. 723-736, John Wiley & Sons, Ltd., 2004.